Processing and characterization of hydroxyapatite coatings on titanium produced by magnetron sputtering

doi: 10.1557/JMR.2001.0446

Processing and characterization of hydroxyapatite coatings on titanium produced by magnetron sputtering

T.G. Nieh and A.F. Jankowski
Lawrence Livermore National Laboratory, L-350, P.O. Box 808, Livermore, California 94551-9900
J. Koike
Department of Materials Science, Tohoku University, 02 Aoba-yama, Aoba-ku, Sendai 980-8579, Japan

(Received 30 April 2001; accepted 31 August 2001)

Hydroxyapatite (HA) coatings with different thicknesses were produced on Ti and Si substrates using the radio frequency magnetron sputtering method. The mechanical properties, for example, modulus and hardness, of the coatings were measured using nanoindentation. The measured values of modulus and hardness were close to the upper limit of that reported for bulk HA, indicating a fully dense structure. Interfacial strengths between the HA coatings and substrates were also evaluated using a nanoscratch technique. The HA–Ti interface appeared to be stronger than the HA–Si interface. The microstructures of the HA coating and the HA–Ti interface were examined using high-resolution electron microscopy. Chemical compositions of the HA coating and the HA–Ti interface were also analyzed using x-ray energy dispersive spectrometer and electron energy loss spectroscopy. The results indicated that the strong HA–Ti bonding is associated with an outward diffusion of Ti into HA layer and concomitant formation of TiO_2 at or near the interface.

I. INTRODUCTION

Bone and teeth are mineralized tissues whose primary function is "load bearing." Wet cortical bone is composed of 22 wt% organic matrix, 69 wt% mineral, and 9 wt% water.[1] The major subphase of the mineral consists of submicroscopic crystals of an apatite of calcium and phosphate, resembling hydroxyapatite (HA) crystal structure. The apatite crystals are usually formed as slender needles, 20–40 nm in length by 1.5–7 nm in thickness.[2] Hydroxyapatite $[Ca_{10}(PO_4)_6(OH)_2]$ has the unit cell dimensions of $a = 0.9432$ to 0.9418 nm and $c = 0.6881$ to 0.6884 nm, and the maximum x-ray diffraction plan is (211).[3] The ideal Ca/P ratio of HA is 1.67 and the calculated density is 3.219 g/cm^3.[4] Calcium phosphate-based bioceramics have been in use in medicine and dentistry for over 20 years, because of its excellent biocompatibility with human tissues. Applications of fully dense bioceramics include dental implants, percutaneous devices, and use in periodontal treatment, alveolar ridge augmentation, orthopedics, maxillofacial surgery, otolaryngology, and spinal surgery.[5]

Whereas porous hydroxyapatite has been successfully synthesized for non-load-bearing bioimplants,[6] it is still considered not suitable for load-bearing application because of its low mechanical strength. In contrast, hydroxyapatite coating on metallic implants, e.g., Ti and Co alloys, to improve surface biocompatibility is considered to be an alternative solution. The coating approach is more practical than designing a new monolithic hydroxyapatite structure, since metallic implants have been used for many years and their mechanical responses are well understood. A hydroxyapatite-coated metallic implant is expected to extend its useful life.

Various coating methods, including plasma spray,[7] magnetron sputtering,[8–10] electrodeposition,[11,12] and vapor deposition,[13] have been investigated to produce reliable HA coatings. Each method has its own merits and drawbacks. An ideal HA coating is expected to be fully dense and to have a good adhesion at the coating–Ti interface, to minimize direct Ti–body fluid contact. It must be porous (with a pore size approximately 100–200 μm) at the outer surface to permit tissue ingrowth, which is important for stress transfer during loading. In summary, mechanical and physical considerations lead to the concept of a graded coating, shown in Fig. 1, in which the coating is fully dense at the Ti–HA interface, but the density decreases gradually to about 50% near the surface. That is, it is a graded structure. Also, pores in the coating must be interconnected allowing full circulation of body fluid. Such coating is technologically challenging to produce, and scientifically difficult to model. Plasma spray is a practical and economic way to produce porous structures. However, good

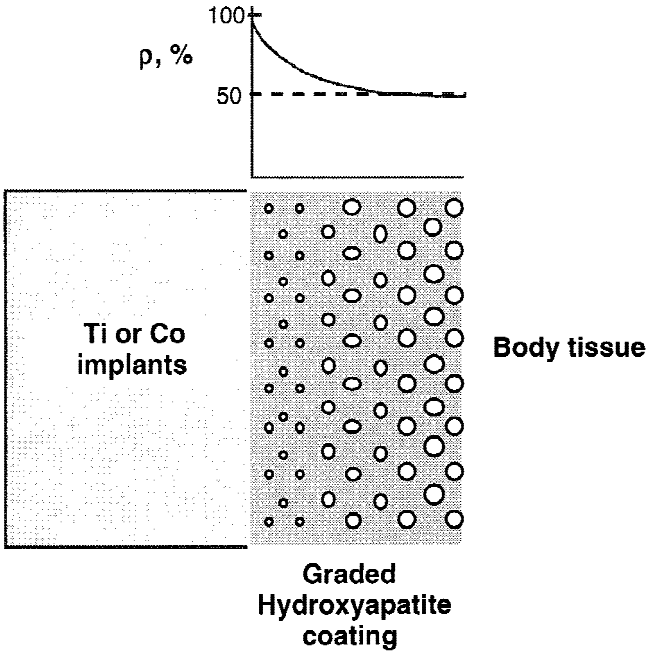

FIG. 1. A desired coating is fully dense at the implant–HA interface to prevent metal–body fluid interaction, but porous (graded) at the HA–tissue interface to allow ingrowth of body tissue.

bonding between the HA coating and metal substrate and the control of the chemical composition of the HA coating are always challenging.[14] One possible way to overcome the bonding problem is to pre-coat a thin HA layer and then overcoat HA with a plasma spray method. In the present study, we produced HA coatings on Ti and Si substrates using a magnetron sputtering technique and further characterize the microstructures and mechanical properties of the coatings. An explanation for the observed good bonding between HA and Ti substrate is offered.

II. SAMPLE PREPARATION AND EXPERIMENTAL PROCEDURES

The coatings used for this investigation were prepared by sputter deposition using planar magnetrons operated in the direct content and radiofrequency (rf) modes. The high vacuum chamber was cryogenically pumped to a base pressure of 6 μPa. Each planar magnetron had a 63-mm diameter and was horizontally positioned at a source-to-substrate separation of 102 mm. The target materials were 99.94% pure titanium and hydroxyapatite, which were produced by hot pressing hydroxyapatite powders, prepared by a precipitation[15] method, in air at 1300 °C. The substrate wafers were polished, single-crystal (111) silicon and wafers that were sputter coated with a 1-μm-thick layer of titanium (denoted as Ti/Si substrate). The substrate table was held at room temperature. The hydroxyapatite coatings were subsequently deposited by magnetrons in the rf at a forward power of 75 W with a working gas pressure of 1.3 Pa at a flow rate of 40 cc min^{-1}. Two coating thicknesses, 0.35 and 0.65 μm, were produced. The 0.65-μm-thick coating was produced using a working gas of pure Argon, whereas in the case of 0.35-μm-thick coating, a working gas mixture of Ar–3%O_2 was used. A 1.5-μm-thick coating was also prepared, but the coating was cracked, apparently resulting from the presence of large residual stresses in the film.

The microstructure of the 0.65-μm-thick HA coating on the Ti/Si substrate was observed with a transmission electron microscope (TEM) equipped with a field-emission electron gun. TEM samples were prepared by mechanical grinding and ion milling. Chemical composition was determined by an x-ray energy dispersive spectrometer (EDS) and an electron energy loss spectrometer (EELS), both attached to the TEM. A nominal probe with a diameter of 7 nm was used for the analysis. To obtain reliable information about the concentration, both spectrometers were used in a complementary manner. The EDS was capable of analyzing Ca and P, but not O. On the other hand, the EELS was capable of analyzing Ca and O, but not P. This was because the P loss peak appeared at 135 eV with a very strong background intensity of a plasmon peak. To estimate Ca/P ratio in the coating, Rutherford backscattering spectrometry (RBS) was also carried out with 2.3-MeV He^+ ions for analysis. The RBS measurements were performed on a 0.5-μm-thick HA coating on Si substrate with the ion beam at normal incidence and at 60° off normal, which doubles the path length and the beam spot area.

Nanoindentation tests were performed on the coated samples with a Š. Nano Indenter XP (Nano Instrument, Oak Ridge, TN). Hardness and elastic modulus were measured by the continuous stiffness option, which yields elastic modulus and hardness as a function of indentation depth. A Berkovich indenter was used in the experiments. A quartz sample was used as a standard for the initial calibration. Five types of experiments—hardness test at a load, hardness test at a depth, continuous stiffness test at a depth, continuous stiffness at a load, and a four times load/unload experimental procedure—were performed at different loads and depths. Ten indentations were made for each test on each specimen, with most of the results presented here representing averages for the group. To provide a measure of scratch resistance or adhesive strength of the coatings, ramping load scratch tests were performed on samples over a 500-μm length.[16,17] During testing, the applied normal load was linearly increased from an initial 20 μN to the maximum loads of 20, 40, 80, and 150 mN. The scratched lines were subsequently examined using scanning electron microscopy (SEM).

III. RESULTS AND DISCUSSION

A. Mechanical properties

1. Modulus and hardness

The modulus and hardness as a function of indentation depth of the 0.65 and 0.35-μm HA coatings on Ti/Si and Si substrates are shown in Figs. 2(a) and 2(b), respectively. The indentation measurements on the 0.65-μm coating were terminated at a depth of 220 nm, which is about a third of the total HA coating thickness. The initial drops in both modulus and hardness in Figs. 2(a) and 2(b) were associated with an uncertainty in determining contact area of the indenter upon the initial nanoindentation. After the initial drop, both the modulus and hardness are noted to increase gradually with increasing indentation depth. The increases are caused by the harder substrates, Si and Ti. [The modulus and hardness of Si (111) are about 160 and 13 GPa respectively,[18] and the modulus of Ti is about 116 GPa]. However, the modulus and hardness of the HA coatings are estimated to be about 120 and 7.8 GPa, respectively. This hardness value is slightly higher than that of the HA target (fully dense HA), which is about 6.5 GPa. The measured modulus and hardness of the HA coating on the Ti/Si substrate are noted to be slightly lower than that measured from the coating on the Si substrate. This is a result of the fact that Si is stiffer and harder than Ti. In comparison, the modulus of monolithic bulk HA, depending upon its density, has been reported to be between 41 to 121 GPa.[19] The modulus of the present coatings is therefore near the high end of the spectrum, suggesting a high-density material. The modulus of the present coating is much higher than that of a natural bone, which is only 7–25 GPa.

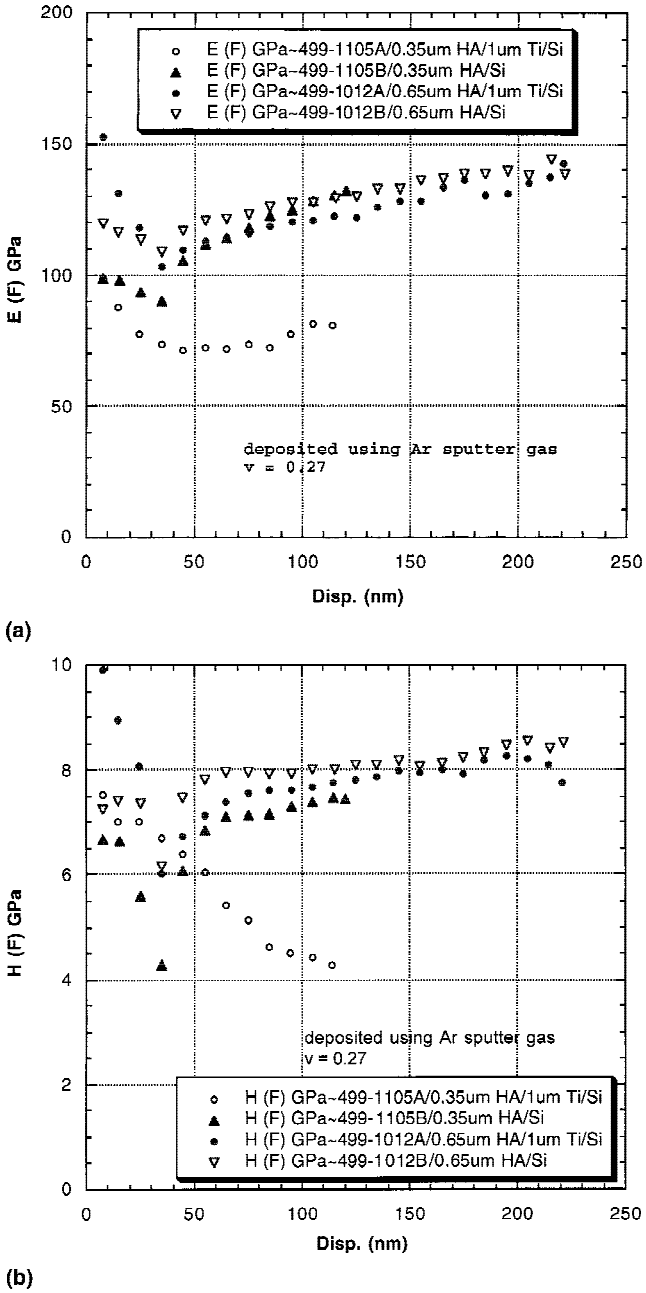

FIG. 2. (a) Modulus and (b) hardness of HA coatings on Ti/Si and Si substrates. The measured modulus and hardness are similar for different substrates. The continual increase in both modulus and hardness values with indentation depth are attributed to hard substrates.

2. Scratch test

To evaluate the interfacial cohesion between HA coating and substrates, the ramping load nano-scratch technique was performed. The ramping normal load of 0.02–20 mN was used for a scratch distance of 500 μm. Scratch and surface profiles both before and after scratch of the 0.65-μm-thick HA coating on the Ti/Si substrate are shown in Fig. 3(a). For easy discussion, the ramping normal load is also included in the figure (bottom). The prescan profile indicates that the roughness of the sample surface is about 40 nm. The scratch profile is relatively smooth but nonlinear. In fact, the slope of the profile monotonically decreases with increasing depth; this is obviously a result of increasing contact area. The depth difference between the scratch and postscan profiles represents the elastic recovery of the coating and substrate. Identical tests were also carried out with the 0.65-μm-thick HA coating on the Si substrate and the results are shown in Fig. 3(b). As is readily seen, the results are remarkably similar to that obtained from the HA coating on the Si substrate.

Normally, during a ramping load test, sudden changes in the friction coefficient (or load) are often observed, which are associated with microcracking or delamination of the films. The load that causes the delamination is denoted as the "critical load," which provides a quantitative measure of scratch resistance or adhesive strength of a film.[16] However, no sudden increase in the friction coefficient was discernible during scratch tests of HA coatings, as shown in Fig. 3. It is noted in the figure that the total plowing depth is 140 nm, which is about

one-third of the coating thickness; plastic zone caused by scratching may not have reached the interface. Greater maximum loads of 40, 60, 80, 100, and 150 mN were subsequently applied on the HA/Ti sample. However, even with a maximum load of 150 mN, which produces a plowing depth of 900 nm (greater than the thickness of the coating), no abrupt change in friction coefficient was observed, indicating a strong bonding between HA and Ti.

Despite the similar mechanical response, scratch marks on the two coatings are quite different. For the HA/Si sample, a complete film separation was observed [Fig. 4(a)], suggesting a poor HA–Si interfacial bonding. In contrast, for the HA/Ti sample [Fig. 4(b)], the end of scratched HA film still attaches to its substrate. These results indicate a stronger bonding between HA coating and Ti than that between HA and Si.

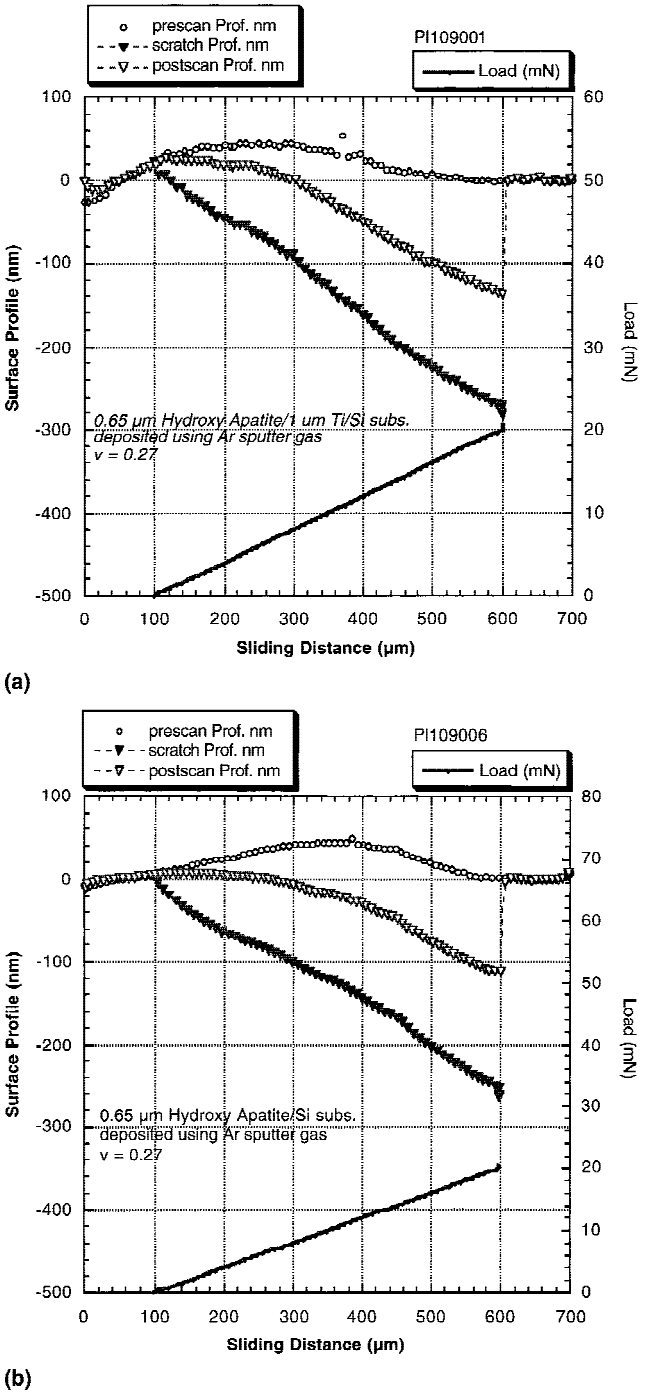

FIG. 3. (a) Ramping load scratch profiles from HA coating on Ti/Si substrate. The smooth scratch curve (no sudden change in surface profile) suggests no delamination, and thus good adhesion, between substrate and coating. (b) Ramping load scratch profiles from HA coating on Si substrate. The scratch profile is remarkably similar to that observed from HA coating on Si substrate.

B. Microstructure

1. Target material and coating morphology

The grain structure of the hydroxyapatite target revealed by SEM is shown in Fig. 5. It is nearly fully dense (approximately 99.7%), with small pores distributed

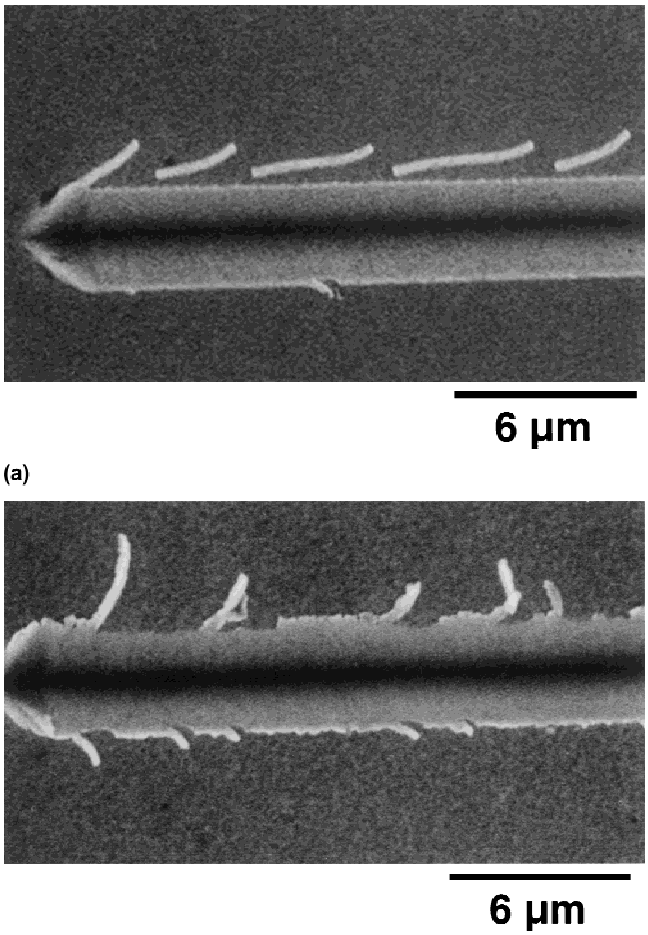

FIG. 4. Scratch morphology of HA coating on (a) Si and (b) Ti/Si substrate. Scratch marks on the two coatings are apparently different. Scratched HA film in the HA/Ti sample still attaches to its substrate, indicating a stronger bonding between HA coating and Ti than that between HA and Si.

primarily along grain boundaries and triple junctions. It is a two-phase structure with a mean grain diameter of about 4 μm. X-ray analysis indicates that the sample contains, in addition to hydroxyapatite, a small amount (less than 5%) of tri-calcium phosphate (TCP). This is somewhat expected since apatite is essentially a line compound, and thus is technically difficult to obtain in the pure form. The hardness of this hydroxyapatite is about 6 GPa. Figure 6 shows a bright-field TEM image of the hydroxyapatite target. The image reveals equilibrated, hexagonal-shaped grains with sharp apexes and a mean grain size of approximately 3 μm. The Ca/P ratio of the sputter target was analyzed by energy dispersive x-ray (EDX) and was found to be essentially a constant.

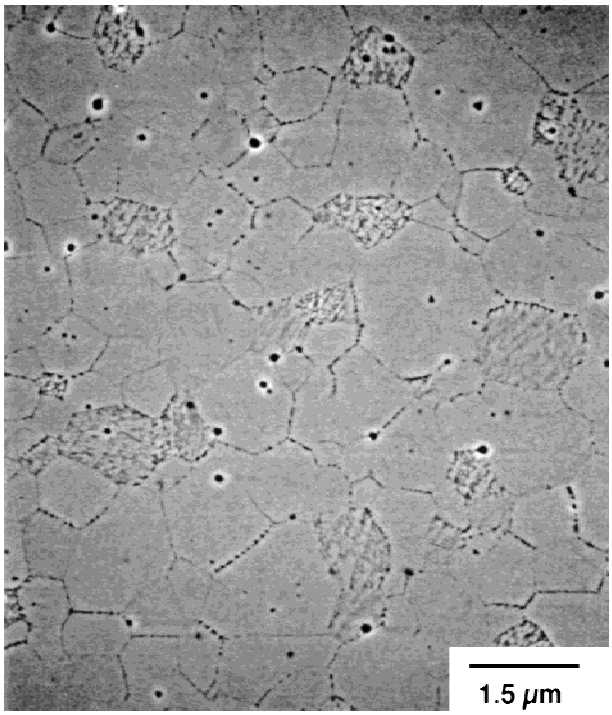

FIG. 5. SEM micrograph shows an equilibrated, equiaxed structure in the fully dense HA.

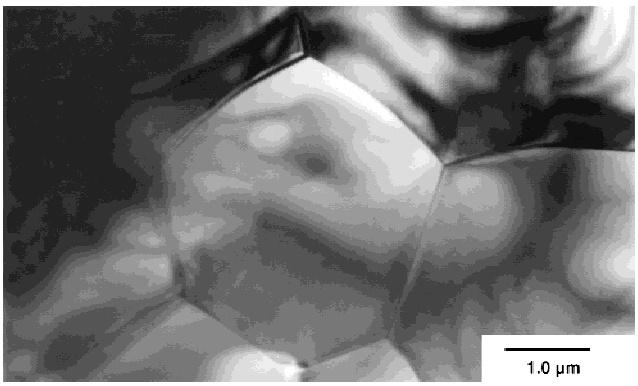

FIG. 6. TEM micrograph shows the fine-grained structure of fully dense HA target.

Sputter coating of HA with pure Ar gas produces samples with a smooth surface. In contrast, samples prepared with an oxygen/argon mixture are relatively rough. Numerous bubbles with sizes of about 1–5 μm were observed (Fig. 7). The presence of these bubbles suggests that some gaseous species were trapped in the coating. The fact that no bubbles were observed in coatings prepared with pure Ar gas indicates that oxygen-containing gas causes the bubble formation. It is noted that oxygen gas may also chemically react with Ti or Si substrate in the initial stage of deposition. Such a reaction is expected to degrade the adhesion of HA and lead to spalling.

As discussed earlier, special efforts were made to deposit 1.5-μm-thick HA coatings. However, it was found that a high density of surface cracks was present in the coatings (Fig. 8). The observed surface cracks are believed to be a result of the presence of exceedingly large residual stresses. The thermal expansion coefficient of HA ($15 \times 10^{-6}\ K^{-1}$) is about 70% higher than that of Ti ($9 \times 10^{-6}\ K^{-1}$), and 3 times that of Si ($5 \times 10^{-6}\ K^{-1}$). This large difference in thermal expansion coefficient can produce a significant residual stress in thick HA coatings even during a small thermal excursion. The residual stress, whether it is tensile or compressive, can readily lead to surface cracking in brittle ceramics such as HA. Nonetheless, the measured modulus and hardness of the 1.5-μm-thick film are similar to those of the thinner films.

2. Interface structure

A TEM cross-sectional microstructure of the nominal 0.65-μm-thick HA coating on Ti/Si substrate is shown in Fig. 9. The thickness of the Ti layer is found to be about

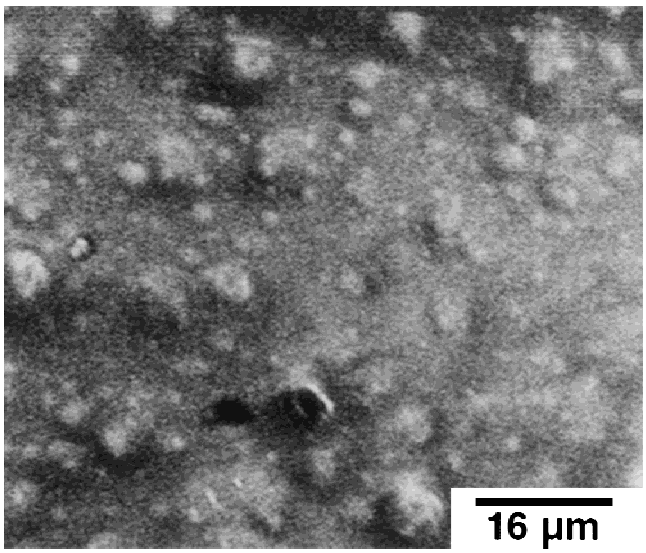

FIG. 7. Bubbles formed on the surface of HA coating produced by using Ar + 3%O_2 gas.

620 nm with an interface roughness of 14 nm. The total thickness of the HA layer, on the other hand, is 735 nm. In comparison to the Ti underlayer, the surface roughness of the HA layer is reduced. The Ti layer consists of columnar grains with a grain size of 70 nm near an interface with the oxide film. The grain size is much smaller in the vicinity of an interface with the Si substrate. The hydroxyapatite layer does not exhibit any diffraction contrast, indicating an amorphous structure. The amorphous structure is further confirmed by a diffraction pattern. Amorphous structure was also observed in the as-deposited HA coatings prepared by magnetron sputtering[10] and evaporation.[13] In contrast, amorphous and crystalline structures were observed in plasma-sprayed samples, presumably from excessive heating.

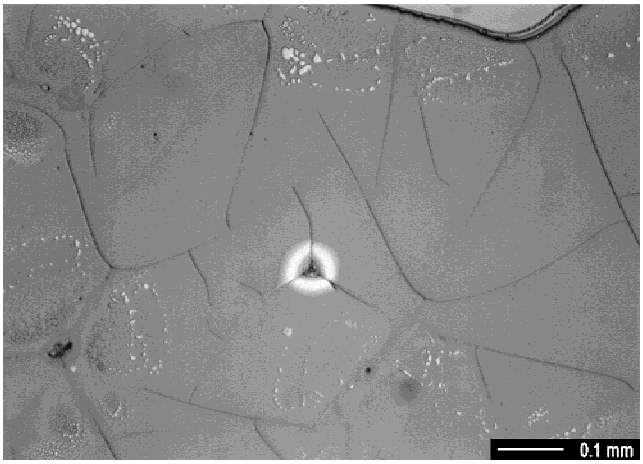

FIG. 8. A cracked 1.5-μm-thick HA film on Ti–Si substrate under indentation. Cracking can be attributed to a large residual stress in the film.

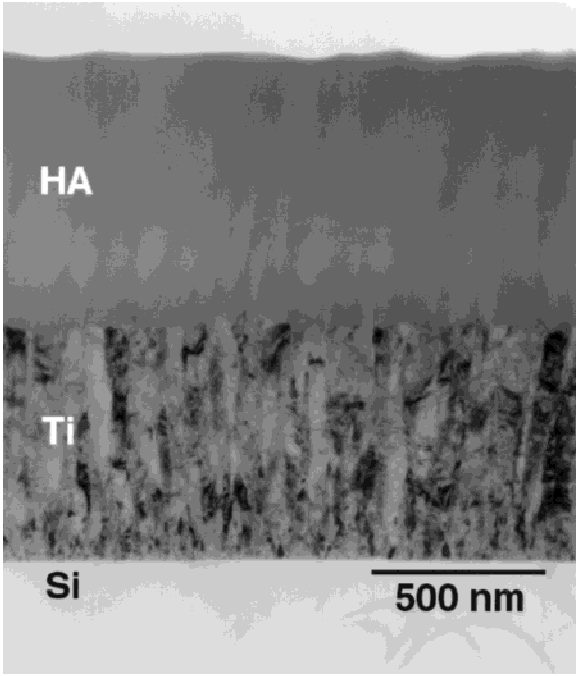

FIG. 9. Cross-section structure of HA coating on Ti/Si substrate. The Ti substrate has a fine-grained columnar structure with a surface roughness of about 14 nm. HA has a uniform amorphous structure.

A high magnification view of the interface region between the Ti and the HA layer is shown in Fig. 10(a). There is no intermediate phase formed at the interface. The interface position is determined based on the presence of lattice fringes in the Ti layer and is indicated by a thin line in the figure. Each black dot indicates a region where an EDS spectrum is taken to determine the Ca/P concentration ratio. Each dot is numbered relative to the EDS results. Region 1 is the Ti layer showing clear lattice fringes. Region 2 is near the Ti–HA interface. Regions 3 and higher are from the HA layer showing the absence of lattice fringes. Corresponding EDS results from these five regions are shown in Fig. 10(b). The number of each probed region is given at the left top corner of each spectrum. It is particularly noted that Ti peaks are observed in the HA layer. The relative intensity of the Ti peaks decreases with increasing distance from the interface. These results indicate that a chemical reaction takes place at the interface caused by the outward diffusion of Ti into the HA layer.

Figure 11 shows EELS spectra from Regions 1 and 3. It is immediately noticed that the spectrum from Region 3 is shifted toward a high energy side with respect to the spectrum of the Region 1. This is known as a chemical shift, which is caused by an increase in binding energy of the core-level electrons. The magnitude of energy shift can be estimated from the difference in an energy-loss value at a half height of a rising edge and is found to be 1.6 eV. This value agrees with a reported value for pure Ti and TiO_2.[20] Furthermore, the spectrum from Region 1 exhibits two sharp peaks related to L2 and L3 lines of pure Ti. In Region 3, on the other hand, these peaks appear to be split, making up a total of four peaks. The peak splitting in Ti has been reported to be a signature of the formation of TiO_2 because of lifting of the degeneracy of Ti 3*d* states by the electrostatic field of oxygen atoms.[20] In the case of TiO_2, however, the magnitude of peak splitting is 2.5 eV. In the present case, it is approximately 1.6 eV. Less splitting may be caused by the fact that the present HA film is amorphous and the electrostatic-field effect from the oxygen atoms is not as strong as in the case of crystalline TiO_2.

It is evident in Fig. 10 that there is extensive outward diffusion of Ti into the HA layer during deposition, even though the substrate is kept at room temperature. The diffusion distance is estimated to be about 50 nm. This is probably, in part, a result of the fact that the structure of the HA is amorphous, which eases the diffusion process. The outward diffusion of Ti and intermixing of Ti and HA is expected to reduce the Ti–HA interfacial

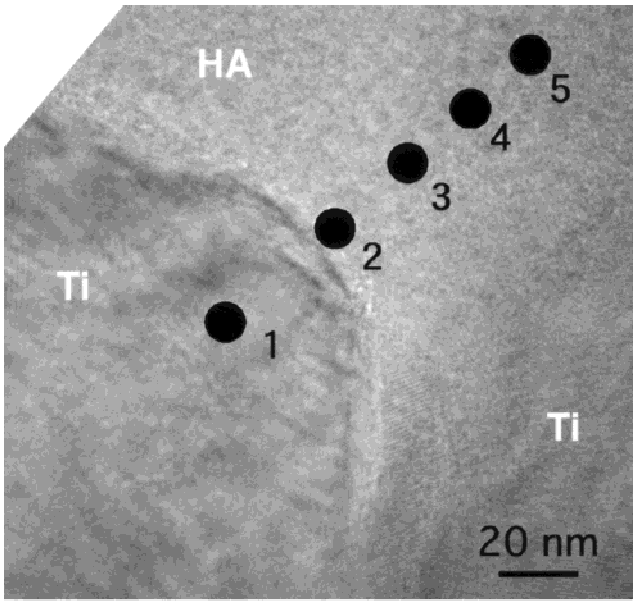

(a)

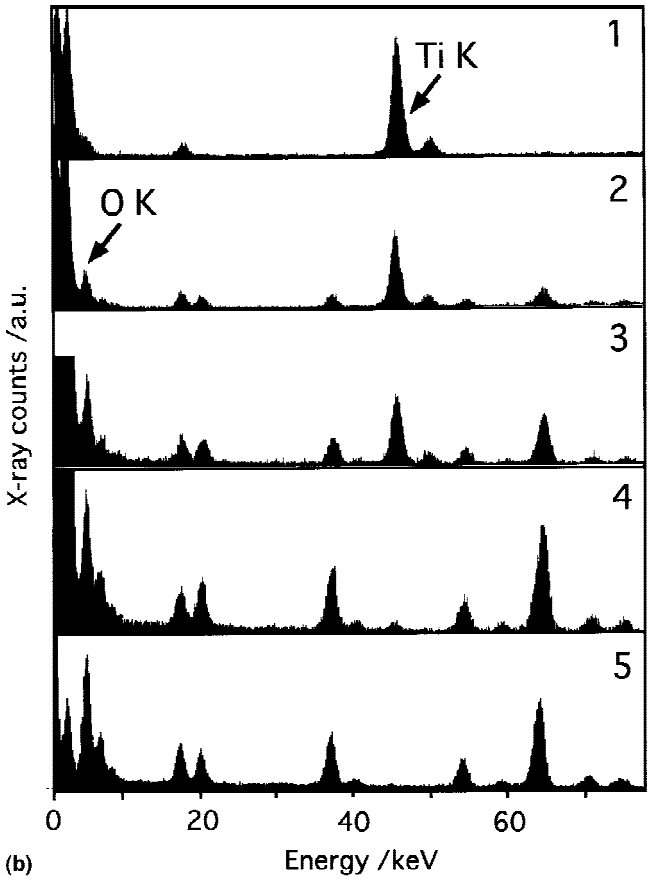

(b)

FIG. 10. (a) A high magnification of cross-sectional structure of HA coating (top) on Ti substrate (bottom two grains). (b) EDAX spectrum from various locations marked in Fig. 10(a), showing the outward diffusion of Ti into HA.

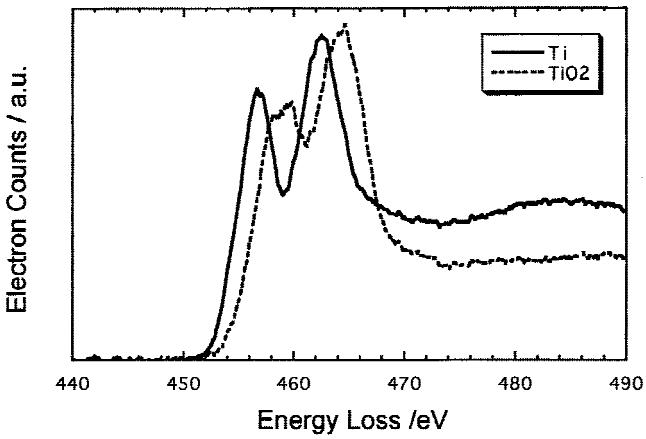

FIG. 11. ELLs spectrum from locations 1 and 5 in Fig. 10(a), showing the chemical shift and crystal split of Ti.

stresses and thus improve the bonding. This is similar to the situation of having a Ti–HA functionally graded structure, in which improved strength and toughness were observed.[21]

It is noted that the Ti–HA interface is slightly rough, with a roughness of about 14 nm (Figs. 9 and 10). However, the rough interface is not expected to contribute significantly to interfacial shear strength. In summary, good bonding between the HA coating and Ti substrate is not caused by a direct chemical reaction between the two materials per se, but rather an outward diffusion of Ti into HA, which results in a graded structure, and the concomitant formation of TiO_2 near the interface.

The Ca/P ratio determined from EDS and EELS is 1.41, which is less than the expected value of 1.67 from a stoichiometric HA. This is probably in part caused by preferential sputtering of lightweight P atoms with respect to heavy Ca atoms. The Ca deficiency is consistent with a previous result of van Dikj *et al.*[9] who also used the rf magnetron sputtering technique to deposit HA. The Ca/P ratio in their coatings was found to decrease with decreasing sputtering input power. For example, it is 2.2–2.4 at an 800W input power but reduces to 1.7–1.8 at a 200W input power. The power used in the present study was only 75W and thus expected to produce a lower Ca/P ratio than the theoretical value of 1.67.

IV. SUMMARY

Thin hydroxyapatite coatings (0.35 and 0.65 μm thick) were produced by rf magnetron sputtering on both Si and Ti/Si substrates. The Ca/P ratio in the coatings was lower than the theoretical value of 1.67, which attributable to a low sputter input energy. Nanoindentation tests showed that the modulus of the coating was about 120 GPa, which is close to the value for the fully dense bulk hydroxyapatite. The hardness was about 8 GPa, which is

higher than 6.5 GPa for a fully dense HA. Ramping load scratch tests were also performed, and the results indicated a strong bonding between HA and Ti but poor bonding between HA and Si. Microstructural and chemical analyses across the HA–Ti interface revealed the presence of Ti and TiO_2 in HA coating. It is therefore proposed that the strong bonding between the HA coating and Ti substrate is not caused by a direct chemical reaction between the two materials per se, but a result of outward diffusion of Ti into HA layer and the concomitant formation of TiO_2 near the interface. In the present study, it was also demonstrated that a thick HA coating (e.g., 1.5 μm) could lead to surface cracking, probably caused by a large thermal expansion mismatch between the two materials.

ACKNOWLEDGMENTS

This work was performed under the auspices of the United States Department of Energy by Lawrence Livermore National Laboratory under Contract No. W-7405-Eng-48. The authors want to thank Dr. W. Choi for carrying out the nanoindentation tests.

REFERENCES

1. J.T. Triffit, in *Fundamental and Clinical Bone Physiology*, edited by M.R. Urist (Lippincott, Philadelphia, PA, 1980), Chap. 3.
2. H.J. Hohling, B.A. Ashton, and H.D. Koster, Cell Tissue Res. **148,** 11 (1974).
3. A.S. Posner, A. Perloff, and A.D. Diorio, Acta Crystallogr. **11,** 308 (1958).
4. D. McConell, *Apatite: Its Crystal Chemistry, Mineralogy, Utilization, and Biologic Occurrence* (Springer-Verlag, Berlin, Germany, 1973).
5. L.L. Hench, J. Am. Ceram. Soc. **74,** 1487 (1991).
6. E.C. Shors and R.E. Holmes, in *An Introduction to Bioceramics*, edited by L.L. Hench and J. Wilson (World Scientific, Singapore, 1993), p. 181.
7. D.M. Liu, H.M. Chou, and J.D. Wu, J. Mater. Sci.: Medicine **5,** 147 (1994).
8. J.G.C. Wolke, K. van Dijk, H.G. Schaeken, K. de Groot, and J.A. Jansen, J. Biomed. Mater. Res. **28,** 1477 (1994).
9. K. van Dijk, H.G. Schaeken, C.H.M. Maree, J. Verhoeven, J.G.C. Wolke, F.H.P.M. Habraken, and J.A. Jansen, Surf. Coating Technol. **76–77,** 206 (1995).
10. K. van Dijk, H.G. Schaeken, J.G.C. Wolke, and J.A. Jansen, Biomater. **17,** 405 (1996).
11. H. Dasarathy, C. Riley, H. Coble, W. Lacefield, and G. Maybee, J. Biomed. Mater. Res. **31,** 81 (1996).
12. M. Wei, A.J. Ruys, M.V. Swain, S.H. Kim, B.K. Milthorpe, and C.C. Sorrell, J. Mater. Sci.: Medicine **10,** 401 (1999).
13. M. Hamdi, S. Hakamata, and A.M. Ektessabi, Thin Sol. Films. **377–378,** 484 (2000).
14. K.A. Khor, Z.L. Dong, C.H. Quek, and P. Cheang, Mater. Sci. Eng. A **281,** 221 (2000).
15. P. Luo and T.G. Nieh, Biomater. **17,** 1959 (1996).
16. B. Bhushan, *Handbook of Micro/Nano Tribology*, edited by B. Bhushan (CRC Press, Boca Raton, FL, 1995), p. 321.
17. J.G. Wang, B.W. Choi, T.G. Nieh, and C.T. Liu, J. Mater. Res. **15,** 913 (2000).
18. T.C. Chou, T.G. Nieh, S.D. McAdams, and G.M. Pharr, Scripta. Metall. Mater. **25,** 2203 (1991).
19. H. Kawahara, in *Ceramics in Surgery*, edited by P. Vincenzini (Elsevier, Amsterdam, The Netherlands, 1982), p. 49.
20. R.D. Leapman, L.A. Grunes, and P.L. Fejes, Phys. Rev. B. **26,** 614 (1982).
21. C. Chenglin, Z. Jingchuan, Y. Zhongda, and T. Shidong, Mater. Sci. Eng. A **271,** 95 (1999).